

# Automatic Kernel Generation for Volta Tensor Cores

Somashekaracharya G. Bhaskaracharya  
NVIDIA  
sbhaskaracha@nvidia.com

Julien Demouth  
NVIDIA  
jdemouth@nvidia.com

Vinod Grover  
NVIDIA  
vgrover@nvidia.com

**Abstract**—A commonly occurring computation idiom in neural networks is to perform some pointwise operations on the result of a matrix multiplication. Such a sequence of operations is typically represented as a computation graph in deep learning compilers. When compiling to a GPU target, these computations can be individually mapped to manually tuned implementations provided by libraries such as cuBLAS and cuDNN. These libraries also provide off-the-shelf support for targeting tensor cores in NVIDIA GPUs, which can lead to huge performance boosts through their specialized support for mixed-precision matrix math. Alternatively, tensor cores can be programmed directly using CUDA APIs or inline assembly instructions, which opens up the possibility of generating efficient CUDA kernels automatically for such computations.

Automatic kernel generation is particularly crucial when it is beneficial to generate efficient code for an entire computation graph by fusing several operations into a single device function instead of invoking a separate kernel for each of them. Polyhedral compilation techniques provide a systematic approach for the analysis and transformation of a sequence of affine loop-nests. In this paper, we describe a polyhedral approach to generate efficient CUDA kernels for matrix multiplication using inline assembly instructions for programming tensor cores on NVIDIA Volta GPUs. Furthermore, we build on this approach to generate fused kernels for computation sequences involving matrix multiplication and pointwise operations such as bias addition, ReLU activation etc. Experimental evaluation of these techniques show that automatically generated kernels can provide significantly better performance than manually tuned library implementations, with speedups ranging up to  $2.55\times$ .

**Index Terms**—matmul, polyhedral compilation, tensor cores

## I. INTRODUCTION

Tensor cores in NVIDIA GPUs are processing cores specialized for matrix operations. They provide huge boosts in throughput and efficiency by performing several mixed-precision matrix-multiply and accumulate calculations in a single operation. Consequently, tensor cores can significantly speed up generalized matrix-multiply (GEMM) and convolutions (as implicit GEMMs), both of which are used heavily in deep learning systems and other computational applications. CUDA libraries such as cuBLAS [1] and Cutlass [2] provide off-the-shelf support for leveraging tensor core capabilities through manually tuned implementations of GEMM for various input matrix layouts (row-major and column-major). Furthermore, cuDNN [3] is a widely used GPU-accelerated library with extensive support for various deep learning primitives.

Deep learning computations can be modeled as dataflow graphs where each node represents a specific computation

such as matmul, convolution, pointwise operations etc. A commonly occurring computation idiom in neural networks is that of a matmul feeding a bias add, which then drives an activation function such as ReLU. These computations can be specified through various deep learning frameworks such as TensorFlow [4], PyTorch [5]. A naive approach to map these computations onto a GPU would invoke separate kernels for each computation node in an execution order dictated by the dataflow dependences. However, the repeated round-trip through global memory is inefficient and can be eliminated if multiple operations are fused into the same kernel. So, for the above example, the entire computation should be ideally mapped to a single kernel that performs matmul as well as its downstream pointwise operations, without the overhead of writing the intermediate results to global memory. In this context, it is imperative to explore kernel generation techniques not just for matmul but also for matmul with such pointwise operations in its epilogue or prologue i.e., downstream or upstream to it in the computation graph.

Automatic kernel generation for tensor cores requires direct programmatic access to tensor cores. On a Volta GPU, tensor cores can be programmed directly using the `mma.sync.m8n8k4` PTX instruction [6] for half-precision floating point type. The operation is defined for each quad-pair, i.e, a group of 8 threads. The `mma.sync.m8n8k4` instruction for half-precision floats (the `fp16` data type) on Volta requires each thread in a quad pair to own fragments of the input matrix to a matrix multiply-and-accumulate operation. Each fragment consists of 4 half-precision floats. Consequently, the input fragments from all the threads in a quad-pair constitute the two  $8\times 4$  and  $4\times 8$  input matrices for the matrix-multiply-and-accumulate operation (mma). The resulting  $8\times 8$  matrix is distributed across the quad-pair's threads, and each thread owns a piece of the accumulator matrix called the accumulator fragment, which is of size  $1\times 8$ .

Another way to program tensor cores is through the wmma CUDA APIs [7]. Unlike an `mma.sync.m8n8k4` instruction, the wmma operation is defined for an entire warp. A wmma fragment distribution is opaque, and is target dependent. On the other hand, the distribution of `mma.sync` fragments is pre-defined and not target architecture dependent. Furthermore, as we shall see later, the `m8n8k4` mma operation can be composed into higher-order macro-MMA operations in a number of ways to take advantage of wider loads and stores at every level

of the memory hierarchy. Due to this low-level control, the `mma.sync.m8n8k4` instruction lends itself well to implement efficient kernels for deep learning graphs, with ample scope for kernel fusion.

Our focus is on generating efficient kernels for computation graphs that involve matmul and pointwise operations such as add, subtract, and activation functions such as ReLU, Sigmoid and Tanh. In particular, the scope of this work is restricted to the following computation idioms.

- matmul without any epilogue or prologue
- matmul with pointwise operations in its prologue
- matmul with pointwise operations in its epilogue
- matmuls of the same shape feeding a pointwise operation

These operations can be expressed as affine loop-nests. Polyhedral frameworks have proven to be effective for analyzing and transforming a sequence of affine loop-nests [8]–[10]. Several deep learning compiler frameworks [11]–[13] support polyhedral compilation techniques in conjunction with other analysis tools and intermediate representations. In this paper, we describe a polyhedral approach to automatically generate efficient kernels for Volta tensor cores given a high-level computation DAG where each node represents a matmul or a pointwise operation such as add, subtract, ReLU, Sigmoid, Tanh. To summarize, our contributions are as follows.

- We describe polyhedral techniques to automatically generate efficient kernels that implement matmul using the `mma.m8n8k4` PTX instruction on a Volta GPU, by composing the `m8n8k4` mma tile into higher-order macro-MMA operations of shapes `m16n16k8` and `m32n32k8` for realizing a warp-level MMA.
- We then build on the above approach to automatically perform kernel fusion for some commonly occurring computation idioms involving matmul and pointwise operations.
- We implement and evaluate our approach for these computation idioms on various problem sizes and demonstrate significant speedups over manually-tuned implementations provided by standard libraries such as cuBLAS and cuDNN.

Section II provides the necessary background and introduces the notation use in later sections. Sections IV, V and VI describe the compute decomposition and data movement required for mapping a matmul computation to Volta tensor cores. Kernel fusion using similar decompositions is discussed in Section VII. Experimental evaluation of these techniques is provided in Section VIII. Related work and conclusions are presented in Sections IX and X respectively.

## II. BACKGROUND

This section provides the notation and background for the techniques we present in the rest of this paper.

### A. Programming Tensor Cores

The GPU compute hierarchy consists of blocks of threads which are organized into warps. Each warp consists of 32

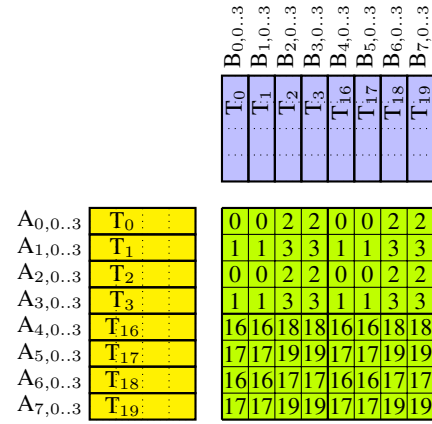


Fig. 1: The shape and data distribution for an `mma.sync.m8n8k4.row.col` operation. Matrix A is row major while matrix B is column major.

threads. These threads can be further partitioned into 8 *quads*, i.e., threads 0–3, 4–7, 8–11, 12–15, 16–19, 20–23, 24–27, 28–31 respectively. A Volta `mma.sync.m8n8k4` instruction is executed by a pair of quads. For example, threads 0–3 and 16–19 constitute quad-pair  $QP_0$ ; threads 4–7, 20–23 constitute quad-pair  $QP_1$  and so on.

As shown in Figure 1, each mma operation is of shape `m8n8k4`, i.e., input matrices of shape  $8 \times 4$  and  $4 \times 8$  are multiplied and added to an accumulator matrix of shape  $8 \times 8$ . The elements in the input matrices are half-precision floats (`fp16` type) whereas the accumulator matrix elements are of type `fp32` (a version of `mma.m8n8k4` with `fp16` accumulators also exists on Volta, although we consider the `fp32` version in this paper). The input matrices can be in either row or column major format with different specializations of the instruction provided for different layout combinations. Each thread in a quad pair owns an input data *fragment*, which is nothing but 4 half-precision floating point values. As shown in Figure 1, thread 0 owns 4 contiguous `fp16` values from the first row and column of the input matrices A and B respectively; thread 1 owns the second row and column and so on. Furthermore, each thread owns an *accumulator fragment*, which consists of 8 elements from the accumulator matrix. In Figure 1, the thread indices specified in the cells of the  $8 \times 8$  accumulator matrix indicate the distribution of the data elements among the different threads.

Finally, with each quad-pair performing a single mma operation, an entire warp can perform 4 mma operations, each of shape `m8n8k4`. More details on the `mma.sync.m8n8k4` instruction in Volta can be found in the CUDA toolkit documentation [6].

### B. Polyhedral Model

Polyhedral model is a mathematical representation of affine loop-nests, where the loop bounds and array access expressions are affine combinations of enclosing loop iterators and program parameters. In the polyhedral representation each execution instance of a statement  $S$  is represented as an

integer point within a polyhedron. The faces of the polyhedron correspond to the bounds on the enclosing loops and the dimensionality of the polyhedron is nothing but the number of enclosing loops. The integer points within the polyhedron capture the iteration domain  $I_S$  of the statement. Each statement may access arrays whose dataspace can also be similarly defined as polyhedra. Consequently, an access relation  $I_S \rightarrow A$  mapping an iteration domain  $I_S$  to a dataspace  $A$  can be used to specify accesses to array  $A$  performed by a statement  $S$ . Similarly, relations between iteration spaces represent RAW, WAR and WAW dependences. Furthermore, the execution schedule of the statement instances is specified by mapping the execution instances to multi-dimensional logical timestamps, whose lexicographic ordering gives the execution order.

The Integer Set Library (ISL) [14] can be used to represent and manipulate such a polyhedral representation. Given the polyhedral representation of a loop-nest or a sequence of loop-nests, the polyhedral scheduler in ISL can be used to determine a valid schedule, such that all dependences are satisfied. ISL also provides facility for manipulating a schedule through its schedule tree representation [15].

### III. PROBLEM STATEMENT

Our focus is on automatic kernel generation for computation DAGs where the nodes represent matmul or pointwise operations. Since each of these operations can be specified as affine loop-nests, each node also encapsulates its corresponding polyhedral representation – the iteration space, data space, access relations as well as the dependence relations. Such a computation DAG serves as the input to our kernel generation problem. DSLs such as Halide [16], Tensor Comprehensions [11] can be used to derive such a DAG.

```

1 for(i = 0; i < M; ++i)
2   for(j = 0; j < N; ++j)
3     for(k = 0; k < K; ++k)
4 /*S1*/ C[i, j] = mul_acc(C[i, j], A[i, k], B[k, j]);
5
6 for(i = 0; i < M; ++i)
7   for(j = 0; j < N; ++j)
8 /*S2*/ E[i, j] = relu_add(C[i, j], bias[i, j]);

```

Listing 1: Matmul + Bias + ReLU

Listing 1 shows an example where the matmul result is fed to pointwise operations – bias add followed by the ReLU activation function. Each loop-nest maps to a separate node in the computation DAG. Now, the polyhedral model would consist of the following.

- The iteration domains,  $I_1$  and  $I_2$ , for the statements  $S_1$  and  $S_2$ .
- Dataspaces,  $M_C$  and  $M_E$ , written to by  $S_1$  and  $S_2$  respectively.
- Write access relations,  $I_1 \rightarrow M_C$  and  $I_2 \rightarrow M_E$ , specifying write accesses performed on  $M_C$  and  $M_E$  respectively.
- Read access relations,  $\{I_1 \rightarrow M_C, I_1 \rightarrow M_A, I_1 \rightarrow M_B, I_2 \rightarrow M_{bias}, I_2 \rightarrow M_C\}$ , specifying the read accesses performed on the dataspace  $M_C, M_A, M_B$  and  $M_{bias}$  respectively.

- RAW dependences, which consist of both intra-node and inter-node dependences.

Additionally, to facilitate code generation, the following attributes about each statement are tagged on to its iteration space.

- *Expression Tree*. The operations that are to be performed as part of the statement are encoded in the form of an expression tree. Each internal node in the expression tree corresponds to an operation. The result of the root operation is written to the output dataspace. In Listing 1, statement  $S_2$  performs a bias add and ReLU activation, represented by the compound operation `relu_add`. Its expression tree consists of two operations – ReLU and add, with ReLU as the root operation.
- *Write and read access relations*: These are the leaves of the expression tree and are used to determine the data accesses performed by a statement instance, thereby providing the operands for the parent operation nodes in the tree.

In the following sections, we first discuss the problem of generating efficient Volta kernels for matmul and then build on this approach to generate fused kernels for longer computation sequences.

### IV. MATMUL COMPUTE DECOMPOSITION

The ISL scheduler gives an outer-parallel schedule, which is a good starting point for mapping the computation to a GPU. The matmul loop in Listing 1 has such a schedule. We now describe the compute decomposition for mapping this 3-d loop nest to the GPU compute hierarchy of blocks, warps and threads in order to target tensor cores.

#### A. Macro-MMA

MMA operations with the shape  $m8n8k4$  are defined for a quad-pair. But they can be composed into higher-order macro-MMA operations that are performed by an entire warp. Two such macro-MMA compositions that we employ are of shapes  $16 \times 16 \times 8$  and  $32 \times 32 \times 8$ .

Consider Figure 2 which illustrates the  $16 \times 16 \times 8$  macro-MMA where each warp performs a  $16 \times 16 \times 8$  matrix multiply-and-accumulate operation. The input matrices  $A$  and  $B$  are of size  $16 \times 8$  and  $8 \times 16$  respectively. The accumulator matrix is of size  $16 \times 16$ . As with  $mma.m8n8k4$ , the input matrices may be in row or column major layout, which determines how the input matrices are distributed across the threads. Figure 2 shows the distribution for a scenario where the input matrix  $A$  is row-major and matrix  $B$  is column-major. We refer to the subset of data elements owned by a given thread as a *macro-MMA fragment*. Each input macro-MMA fragment consists of 8 *fp16* values – for example, thread 0 owns the 8 elements in the first row of matrix  $A$  as well as the 8 elements in the first column of  $B$  (note that these elements are also owned by threads 8 and 4 respectively). The accumulator fragment consists of 8 *fp32* values. In Figure 2, the numbers inside the cells indicate the threads that own the corresponding elements in the output matrix. For example, thread 0 owns the first two

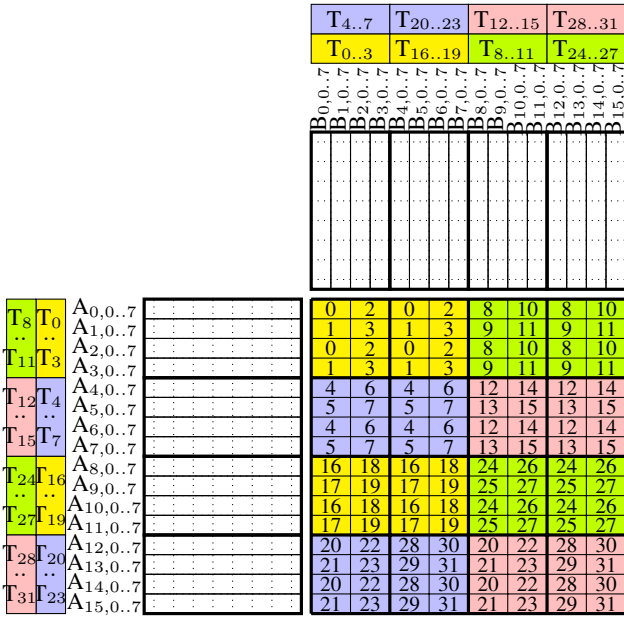


Fig. 2:  $16 \times 16 \times 8$  macro-MMA for row-major matrix A and column-major matrix B.

elements in the first row as well as 3 other pairs of adjacent elements, all of which make up its accumulator fragment. The 4 different colours represent the 4 quad-pairs, thereby indicating the thread-to-data mapping for all the matrices. Regardless of the layout of the input matrices, the distribution of the accumulator matrix for the macro-MMA remains the same.

In case of  $32 \times 32 \times 8$  macro-MMA an accumulator matrix of size  $32 \times 32$  is computed using input matrices of size  $32 \times 8$  and  $8 \times 32$ . An input macro-MMA fragment for a  $32 \times 32 \times 8$  macro-MMA contains 16 *fp16* values, and 32 *fp32* values in its accumulator fragment. Both of these macro-MMA compositions along with wide loads and stores can lead to performance comparable with that of hand-tuned kernels. In the following sections, without any loss of generality, we discuss our approach using  $16 \times 16 \times 8$  macro-MMA as the reference. A similar approach holds good for  $32 \times 32 \times 8$  macro-MMA as well.

### B. Tiling for Blocks and Warps

The outer-parallel schedule obtained using ISL is shown in Figure 3, in the schedule tree form. It corresponds to a 3-d loop-nest and consists of a single permutable band with 3 schedule dimensions. Only the innermost dimension is sequential.

Suppose we distribute the loop-nest across a 2-d grid of size  $b_1 \times b_2$  with each thread block having a 2-d  $w_1 \times w_2$  arrangement of warps. Furthermore, suppose the sequential loop is to be strip-mined with a strip size of  $b_s$ . This can be achieved by successively tiling the loop-nest, first with tile sizes  $b_1 \times b_2 \times b_s$  and then with tile sizes  $w_1 \times w_2 \times b_s$ . We refer to the former as the *block tile* and the latter as the *warp tile*. Clearly, the block tile sizes along every dimension must

exceed or equal the warp tile sizes along the corresponding dimension. Also, they must be integer multiples of the macro-MMA sizes chosen –  $16 \times 16 \times 8$  or  $32 \times 32 \times 8$ . The problem sizes are assumed to be multiples of the block tile sizes. For other problem sizes, we can either pad the input matrices with zeroes to make them so or generate specialized code for the partial tiles and then combine the results of the full-tile computed using macro-MMA and the results of the partial-tiles.

Figure 4 shows the block and warp-level tiling transformation on the schedule tree using tile sizes  $128 \times 128 \times 32$  and  $64 \times 64 \times 32$  respectively. Note that in all three band nodes of the resulting schedule tree, only the innermost dimension is sequential. Clearly, the parallel dimensions of the outermost band correspond to the block indices, *blockIdx.y* and *blockIdx.x*. Similarly, the middle band essentially iterates over the warp tiles. So, its parallel dimensions correspond to warp indices, *warpIdx.y* and *warpIdx.x*, which can be derived from other kernel parameters such as thread indices. Figure 5 shows the schedule tree after these schedule parameters have been introduced.

### C. Strip Mining the Warp-Level MMA

The innermost band in Figure 5, which performs a warp-level MMA operation, processes a warp tile of size  $64 \times 64 \times 32$ . As shown in Figure 6, the sequential dimension in the innermost band can be strip-mined further using a strip size of 8, which corresponds to the macro-MMA size along the *k* dimension. Such a restructuring essentially expresses the warp-level MMA as an outer product, which exposes more instruction-level parallelism than an inner product formulation. This helps cover the latency from instructions and the memory load at a low occupancy.

### D. Schedule Domain Contraction

At this stage, the innermost band in Figure 6 specifies a 3-d loop nest around the statement *S*, each instance of which performs a scalar matrix-multiply and accumulate operation. To target tensor cores, each statement instance must instead perform a macro-MMA operation (of shape  $16 \times 16 \times 8$  or  $32 \times 32 \times 8$ ). This is done by constraining the schedule domain as shown in Figure 7, where an entire subset of integer points corresponding to a  $16 \times 16 \times 8$  macro-MMA is mapped to a single integer point. The root operation in the expression tree associated with the statement *S* is then altered to one that performs a  $16 \times 16 \times 8$  macro-MMA. This means that the innermost band of the schedule tree would then specify the schedule for a loop iterating over  $16 \times 16 \times 8$  macro-MMA instances instead of scalar multiply-accumulate operations. In effect, this distributes the warp-level iteration space across all the threads of the warp. Note that the updated operation type can be of four different types – one for each of the macro-MMA layout specializations.

At this stage, we assume that the macro-MMA fragments owned by each thread are somehow available for the macro-

DOMAIN :  $S[i, j, k] : 0 \leq i < M \wedge 0 \leq j < N \wedge 0 \leq k < K$   
 BAND:  $S[i, j, k] \rightarrow [i, j, k]$

Fig. 3: Initial schedule for matmul in schedule tree form.

DOMAIN:  $S[i, j, k] : 0 \leq i < M \wedge 0 \leq j < N \wedge 0 \leq k < K$   
 BAND:  $S[i, j, k] \rightarrow [\lfloor i/128 \rfloor, \lfloor j/128 \rfloor, \lfloor k/32 \rfloor]$

BAND:  $S[i, j, k] \rightarrow [\lfloor i/64 \rfloor - 2\lfloor i/128 \rfloor, \lfloor j/64 \rfloor - 2\lfloor j/128 \rfloor, 0]$   
 BAND:  $S[i, j, k] \rightarrow [i - 64\lfloor i/64 \rfloor, j - 64\lfloor j/64 \rfloor, k - 32\lfloor k/32 \rfloor]$

Fig. 4: Tiling with block tile size of  $128 \times 128 \times 32$  and warp-level tile size of  $64 \times 64 \times 32$ .

DOMAIN:  $S[i, j, k] : 0 \leq i < M \wedge 0 \leq j < N \wedge 0 \leq k < K$

BAND:  $S[i, j, k] \rightarrow [blockIdx.y, blockIdx.x, \lfloor k/32 \rfloor]$   
 BAND:  $S[i, j, k] \rightarrow [warpIdx.y, warpIdx.x, 0]$

BAND:  $S[i, j, k] \rightarrow [i - 64\lfloor i/64 \rfloor, j - 64\lfloor j/64 \rfloor, k - 32\lfloor k/32 \rfloor]$

Fig. 5: Introducing kernel parameters –  $blockIdx.y$ ,  $blockIdx.x$ ,  $warpIdx.y$ ,  $warpIdx.x$ .

Fig. 8: Schedule tree transformations for matmul.

DOMAIN:  $S[i, j, k] : 0 \leq i < M \wedge 0 \leq j < N \wedge 0 \leq k < K$   
 BAND:  $S[i, j, k] \rightarrow [blockIdx.y, blockIdx.x, \lfloor k/32 \rfloor]$   
 BAND:  $S[i, j, k] \rightarrow [warpIdx.y, warpIdx.x, 0]$

BAND:  $S[i, j, k] \rightarrow [0, 0, \lfloor k/8 \rfloor - 4\lfloor k/32 \rfloor]$   
 BAND:  $S[i, j, k] \rightarrow [i - 64\lfloor i/64 \rfloor, j - 64\lfloor j/64 \rfloor, k - 8\lfloor k/8 \rfloor]$

Fig. 6: Strip-mining along the  $k$  dimension with strip-size 8.

DOMAIN:  $S[i, j, k] : 0 \leq i < M \wedge 0 \leq j < N \wedge 0 \leq k < K \wedge 16\lfloor i/16 \rfloor = i \wedge 16\lfloor j/16 \rfloor = j \wedge 8\lfloor k/8 \rfloor = k$

BAND:  $S[i, j, k] \rightarrow [blockIdx.y, blockIdx.x, \lfloor k/32 \rfloor]$

BAND:  $S[i, j, k] \rightarrow [warpIdx.y, warpIdx.x, 0]$

BAND:  $S[i, j, k] \rightarrow [0, 0, \lfloor k/8 \rfloor - 4\lfloor k/32 \rfloor]$

BAND:  $S[i, j, k] \rightarrow [i - 64\lfloor i/64 \rfloor, j - 64\lfloor j/64 \rfloor, k - 8\lfloor k/8 \rfloor]$

Fig. 7: Constraining the schedule domain so that each macro-MMA instance is mapped to a single integer point.

MMA operation. In later sections, we discuss how these fragments can be created and loaded with the required data.

### E. Split-K

The compute decomposition described so far parallelizes the matmul computation only along the parallel dimensions, i.e., the  $i$  and  $j$  loops. While the  $k$  dimension is sequential, it is reasonable to parallelize along the  $k$  dimension as well when targeting tensor cores. We refer to such a parallelization as *split-K*. A 2-way *intra-thread-block split-K* splits the computation into 2 parts and assigns them to concurrent warps along the  $z$  axis of the GPU compute hierarchy. The partial results computed by corresponding warps along the  $z$  axis then need to be summed up to obtain the final result for the matmul computation. More generally, it is possible to extend this arrangement to a  $p$ -way *intra-thread-block split-K*, where  $p$  is a power of 2.

1) *Tiling for Intra-Thread-Block Split-K*: For a  $p$ -way split-K, the block tiles need to be bigger by a factor  $p$  along the  $k$  dimension, while the warp tiles are of the same size as before. So, the compute decomposition for a  $p$ -way split-K involves tiling the loop-nest, first with tile sizes  $b_1 \times b_2 \times p \cdot b_s$  and then with  $w_1 \times w_2 \times b_s$ . This creates  $p$  rows of warp tiles along the  $z$  axis of the GPU compute hierarchy. Figure 9 illustrates this approach for a 2-way *intra-thread-block split-K*. Clearly, the resulting schedule in the middle band is for a loop-nest that iterates over warp tiles along the  $y$ ,  $x$  and  $z$  dimensions respectively. So, on introducing these derived kernel parameters, along with the block indices, the schedule tree would be as shown in Figure 10.

The above tilings are followed up with strip-mining and schedule domain contraction as shown earlier in Figures 6 and 7 to complete the compute decomposition for a  $p$ -way split-K.

## V. DATA MOVEMENT ACROSS MEMORY HIERARCHY

In order to obtain good performance on a GPU, it is important to optimize the movement of data across global

memory, shared memory and registers. In this section, we explain how copy statements that move the data across this memory hierarchy are introduced by inserting their associated copy schedule nodes to the transformed schedule tree obtained after compute decomposition.

The read maps,  $I \rightarrow M_A$  and  $I \rightarrow M_B$  capture the read access relation from the iteration domain of the matmul statement  $S$  to the dataspaces  $M_A$  and  $M_B$ , which are only read. The schedule tree transformation described in the previous section effectively maps the iteration space  $I$  to the schedule space  $I'$  with the schedule vector  $(b_y, b_x, c_0, w_y, w_x, c_1, c_2, c_3, c_4, c_5, c_6, c_7)$ . The dimensions  $b_y, b_x, c_0$  correspond to the schedule dimensions of the outermost band in Figure 7;  $w_y, w_x, c_1$  correspond to the schedule dimensions of the band immediately below it and so on.

1) *Global, Shared and Register Data Tiles*: Using the transformation  $I \rightarrow I'$ , we can derive the mappings  $I' \rightarrow M_A$ ,  $I' \rightarrow M_B$  and likewise, the write mapping  $I' \rightarrow M_C$ , which describe the read and the write access relations from the schedule space  $I'$  to the input and output dataspaces respectively. The basic idea is to infer tiles in the global memory that are accessed at block-level and warp-level. Global data tiles that are reused can then be promoted to shared memory data tiles and register tiles, i.e., copied to shared memory or register files and then reused. For each memory promotion, a new statement is introduced to perform this data copy. Furthermore, the access maps can be analyzed to determine the access depth as well as the dimensions of these data tiles. The iteration domain of the copy statement can be derived from the data space of the corresponding data tile. At the inferred access depth, a new schedule node defining a schedule for the copy statement is inserted into the schedule tree. As explained later, in some cases, the copy operation may not be a simple data assignment and may involve a call to helper functions.

### A. Global to Shared Memory

Block-level read maps  $I'_{block} \rightarrow M_A$  and  $I'_{block} \rightarrow M_B$  can be derived from the read access relations  $I' \rightarrow M_A$  and  $I' \rightarrow$



DOMAIN:  $S[i, j, k] : 0 \leq i < M \wedge 0 \leq j < N \wedge 0 \leq k < K$   
 BAND:  $S[i, j, k] \rightarrow [[i/128], [j/128], [k/64]]$

BAND:  $S[i, j, k] \rightarrow [[i/64] - 2[i/128], [j/64] - 2[j/128], [k/32] - 2[k/64]]$   
 BAND:  $S[i, j, k] \rightarrow [i - 64[i/64], j - 64[j/64], k - 32[k/32]]$

Fig. 9: Tiling initial schedule in Figure 3 with block tile size of  $128 \times 128 \times 64$  instead of  $128 \times 128 \times 32$  for 2-way split-K. Warp tile size remains the same –  $64 \times 64 \times 32$ .

DOMAIN:  $S[i, j, k] : 0 \leq i < M \wedge 0 \leq j < N \wedge 0 \leq k < K$

BAND:  $S[i, j, k] \rightarrow [blockIdx.y, blockIdx.x, [k/64]]$   
 BAND:  $S[i, j, k] \rightarrow [warpIdx.y, warpIdx.x, warpIdx.z]$   
 BAND:  $S[i, j, k] \rightarrow [i - 64[i/64], j - 64[j/64], k - 32[k/32]]$

Fig. 10: On introducing kernel parameters –  $blockIdx.y$ ,  $blockIdx.x$ ,  $warpIdx.y$ ,  $warpIdx.x$ ,  $warpIdx.z$ .

Fig. 11: Schedule tree transformations for matmul with 2-way intra-thread-block split-K.

$M_B$  respectively, by projecting out all the dimensions other than those in the outer schedule band, namely,  $(b_y, b_x, c_0)$ . The ranges of these maps determine the data tiles that are accessed by the compute tile  $(b_y, b_x, c_0)$ . Since this data tile is reused by threads within the block with block indices  $(b_y, b_x)$ , it can be promoted to shared memory.

Furthermore, we separate out the global-to-shared copy by splitting it into a global-to-register copy followed by a register-to-shared copy loop. The global-to-register copy loop is set up in such a way that each thread performs 128-bit accesses (8 contiguous fp16 elements) to global memory. Furthermore, this loop to copy data from global memory to registers using vectorized loads is cyclically distributed across all the threads in a thread block. Such a distribution also ensures that global accesses are coalesced.

1) *Swizzled Shared Memory*: In order to ensure that there are no bank conflicts when reading and writing data to and from the shared memory, the data elements in the shared memory tile need to be permuted or *swizzled*. So, unlike the copy from global memory to registers, which is a straightforward copy of an 8-wide vector of *fp16* data values, the copy from registers to shared memory involves the application of a swizzle function. In essence, the 8-wide vector data is stored to a shared memory buffer where the data ordering is different from that in the corresponding global data tile.

The swizzle function, used to compute the offset in the swizzled shared memory allocation, provides a one-to-one mapping from the unswizzled data tile to the swizzled tile in shared memory. Essentially, it maps the offsets of contiguous blocks of 8 *fp16* data values in the unswizzled data tile to an offset in the shared memory allocation for that data tile. The exact implementation of the swizzle function depends on the number of elements per row and column in the swizzled shared array. We also use different helper functions to copy the data to shared memory for each of the 4 combinations –  $A$  or  $B$  in row or column major layout.

### B. Shared Memory to Register Fragments

The access maps  $I'_{warp} \rightarrow M_A$ ,  $I'_{warp} \rightarrow M_B$ ,  $I'_{warp} \rightarrow M_C$  are obtained by projecting out the dimensions  $(c_5, c_6, c_7)$  from  $I' \rightarrow M_A$ ,  $I' \rightarrow M_B$ ,  $I' \rightarrow M_C$  respectively. The ranges of these warp-level access maps determine the input and output data tiles for the warp-level macro-MMA. For the schedule tree in Figure 7, these data tiles would be of size  $64 \times 8$ ,  $8 \times 64$  and  $64 \times 64$  respectively.

1) *Macro-MMA Register Fragments*: Each thread need not own the entire data tile. Recall the schedule domain contraction in Figure 7 which abstracted away the inner point loops. Similarly, these tiles can be contracted to obtain an array of register fragments. For a  $16 \times 16 \times 8$  macro-MMA, the sizes of the array of macro-MMA fragments can be found as follows.

- The 2-d input data tile of  $M_A$  is contracted by factors  $16 \times 8$  if it is row major, and by factors  $8 \times 16$  if it is column major. For example, a given tile of size  $64 \times 8$  can be contracted down to a  $4 \times 1$  array of register fragments.
- The input data tile of  $M_B$  is contracted by factors  $8 \times 16$  if it is row major and by sizes  $16 \times 8$  if it is column major.
- The output data tile for  $M_C$  is contracted by factors  $16 \times 16$  to obtain the array of accumulator fragments.

Each  $16 \times 16 \times 8$  macro-MMA fragment contains 8 *fp16* elements.

2) *Loading Register Fragments*: In order to load the register fragments, a polyhedral schedule can be created for moving the data from shared memory to register fragments. Each register fragment load involves loading 8 *fp16* values from shared memory. The swizzled storage ensures that there are no bank conflicts due to the read accesses to it. The same swizzling function that is used for storing to shared memory is used to obtain the swizzled offset from which to fetch the data vector in the swizzled storage. Again, the data copy is done using vectorized accesses. The macro-MMA thread-to-data mappings for inputs  $A$  and  $B$  are different. Furthermore, it is different for different layouts – row or column major. Also, different load fragment helper functions are needed for each of the 4 possibilities –  $A$  or  $B$  in row or column major layout.

### C. Macro-MMA on Register Fragments

As described in the previous subsection, the register fragments are inferred from the access maps  $I'_{warp} \rightarrow M_A$ ,  $I'_{warp} \rightarrow M_B$ ,  $I'_{warp} \rightarrow M_C$ . Consequently, a mapping from the global dataspace to the data space of register fragments can be inferred. Using these mappings, all accesses to global memory in the statement  $S$  can be altered to access register fragments instead.

### D. Store to Global Memory

The result of a macro-MMA computation goes into an accumulator fragment, which resides in registers. So, a copy of the data from accumulator fragments to global memory is required.

```

1 extern "C" __global__ void __launch_bounds__(256) kern0(int M, int N, int K, const half * __restrict__ M_0, int ldM_0,
2     const half * __restrict__ M_1, int ldM_1, half * __restrict__ M_3, int ldM_3) {
3     ...
4     for (int c2 = -1; c2 < K / 64; c2 += 1) // 2-way split-K
5         if (K >= 64 * c2 + 128) // prefetch data from global memory
6             #pragma unroll for (int c5 = 0; c5 <= 3; c5 += 1) {
7                 (half8&)(private_M_1[(8 * c5)]) = ((half8&)(M_0[(128 * blockIdx.y + 32 * c5 + linearId / 8) * K + (8 * (linearId
8                     % 8) + 64 * c2 + 64) * 1])); // copy data from global memory to registers
9                 (half8&)(private_M_3[(8 * c5)]) = ((half8&)(M_1[(128 * blockIdx.x + 32 * c5 + linearId / 8) * K + (8 * (linearId
10                    % 8) + 64 * c2 + 64) * 1])); // copy data from global memory to registers
11             if (c2 >= 0) // overlap computation with data movement from global memory to registers
12                 #pragma unroll for (int c8 = 0; c8 <= 3; c8 += 1) { // strip-mine the warp-level macro-MMA
13                     #pragma unroll for (int c11 = 0; c11 <= 3; c11 += 1) {
14                         hmma_load_b_col_swizzled(&hmma_M_5[(c11)][(0)][0][0], &shared_mma_M_2[0], (64 * warpIdx_x + 16 * c11), (32 *
15                            warpIdx_z + 8 * c8), 64); // copy data from swizzled shared buffers to register fragments
16                         hmma_load_a_row_swizzled(&hmma_M_4[(c11)][(0)][0][0], &shared_mma_M_0[0], (64 * warpIdx_y + 16 * c11), (32 *
17                            warpIdx_z + 8 * c8), 64); // copy data from swizzled shared buffers to register fragments
18                     // iterate over the macro-MMAs
19                     #pragma unroll for (int c9 = 0; c9 <= 63; c9 += 16) {
20                         #pragma unroll for (int c10 = 0; c10 <= 63; c10 += 16) { // perform macro-MMA (A is row & B is col-major)
21                             hmma_row_col(&hmma_M_6[(c9 / 16)][(c10 / 16)][0][0], &hmma_M_4[(c9 / 16)][(0)][0][0], &hmma_M_5[(c10 / 16)
22                                ][(0)][0][0], &hmma_M_6[(c9 / 16)][(c10 / 16)][0][0]);
23                         if (K >= 64 * c2 + 128) // prefetch data from shared memory
24                             __syncthreads();
25                         #pragma unroll for (int c5 = 0; c5 <= 3; c5 += 1) { // copy data from registers to swizzled shared buffers
26                             hmma_store_shared_b_col_swizzled(&shared_mma_M_2[0], ((half8&)(private_M_3[(8 * c5)])), (8 * c5));
27                             hmma_store_shared_a_row_swizzled(&shared_mma_M_0[0], ((half8&)(private_M_1[(8 * c5)])), (8 * c5));
28                         }
29                         __syncthreads();
30                     }
31                 if (K >= 64) // iterate over accumulator fragments and store results to global mem, rearrange through shared mem
32                     #pragma unroll for (int c4 = 0; c4 <= 3; c4 += 1)
33                         #pragma unroll for (int c5 = 0; c5 <= 3; c5 += 1)
34                             hmma_store_global_after_reordering(&M_3[(64 * warpIdx_y + 128 * blockIdx.y + 16 * c4) * N + (64 * warpIdx_x + 128
35                                * blockIdx.x + 16 * c5) * 1], &hmma_M_6[(c4)][(c5)][0][0], ldM_3, &sharedBuffer[0]);
36             }
37 }

```

Listing 2: Skeleton code for the matmul kernel generated with block tile size  $128 \times 128 \times 32$  and warp tile size  $64 \times 64 \times 32$ .

1) *Reordering through Shared Memory*: The 8 *fp32* data values making up an accumulator fragment do not map to a contiguous block of 8 elements (please refer Figure 2). Furthermore, it is necessary to convert these data values from the *fp32* accumulator type to the *fp16* output type. So, this precludes a straightforward 8-wide vectorized store to global memory. In order to achieve that, the overall strategy is to move the data from the accumulator fragments to global memory, via shared memory. Essentially, shared memory is used as a temporary buffer to exchange and rearrange the accumulator data in registers so that each thread can finally move a contiguous block of 8 *fp16* values to global memory. For example, as shown in Figure 2, thread 0 owns the first two elements  $C_{0,0..1}$  in the first row of the accumulator matrix, as well as the elements  $C_{0,4..5}$ . Likewise, thread 2 owns  $C_{0,2..3}$  and  $C_{0,6..7}$ . Thread 0 packs the 4 elements that it owns into a 4-wide vector of *fp16* values (after converting them from *fp32* to *fp16*), and copies them to a contiguous block in shared memory. Now, if thread 2 does the same and copies its packed data to the adjacent contiguous block of shared memory, thread 0 can then copy back the entire contiguous block of 8 *fp16* values to registers and rearrange them to obtain the correct data order. A similar procedure is employed for all the threads to make sure that the threads own data elements that form contiguous blocks in the global array. Again, the accesses to shared memory are modeled to avoid bank conflicts and to exploit wide loads and stores.

2) *Split-K Reduction*: In case of a split-K schedule, the partial results computed by corresponding warps along the

$z$  axis must be summed up. This is done by adding the partial results once they are stored to shared memory for the reordering described above. The reduction is performed only by the threads in warps with  $warp_z$  equal to 0. Furthermore, this means that the rest of the threads do not perform any store to global memory.

Reordering involves carefully chosen non-affine access patterns. So, all these details, including data conversion and split-K reduction, are hidden behind a helper function that copies data from an accumulator fragment to global memory through the above steps.

### E. Prefetching and Hiding Latency

As explained earlier, the input data for the macro-MMA computation is obtained by copying the data from global memory to shared memory and then from the latter to the register fragments. A prefetching schedule can be obtained by shifting the schedule bands associated with the corresponding copy schedule nodes accordingly. The schedule is further modified so that the global memory access latency is hidden by overlapping it with the macro-MMA computation.

## VI. CODE GENERATION

The AST generation facility provided by ISL is used to emit CUDA code from the schedule tree that results from the compute and data decomposition discussed in the previous sections. Kernel launch parameters, i.e., the grid and block sizes are inferred through the constraints on the corresponding schedule dimensions in the schedule tree. Listing 2 provides a skeleton of the kernel generated using our approach for

```

1 for(i = 0; i < M; ++i)
2   for(j = 0; j < N; ++j) {
3     for(k = 0; k < K; ++k)
4       C[i, j] = mul_acc(C[i, j], A[i, k], B[k, j]); //S1
5     E[i, j] = relu_add(C[i, j], bias[i, j]); //S2
6   }

```

Listing 3: Matmul + Bias + ReLU

DOMAIN :  $S_1[i, j, k] : 0 \leq i < M \wedge 0 \leq j < N \wedge 0 \leq k < K;$   
 $S_2[i, j] : 0 \leq i < M \wedge 0 \leq j < N$   
BAND:  $S_1[i, j, k] \rightarrow [i, j, k]; S_2[i, j] \rightarrow [i, j, K];$   
SEQUENCE  
FILTER:  $S_1[i, j, k]$   
FILTER:  $S_2[i, j]$

Fig. 12: Initial schedule tree for matmul+bias+ReLU

DOMAIN :  $S_1[i, j, k] : 0 \leq i < M \wedge 0 \leq j < N \wedge 0 \leq k < K;$   
 $S_2[i, j] : 0 \leq i < M \wedge 0 \leq j < N$

BAND:  $S_1[i, j, k] \rightarrow [[i/128], [j/128], [k/32]];$   
 $S_2[i, j] \rightarrow [[i/128], [j/128], [K/32]]$   
BAND:  $S_1[i, j, k] \rightarrow [i - 128[i/128], j - 128[j/128], k - 32[k/32]];$   
 $S_2[i, j] \rightarrow [i - 128[i/128], j - 128[j/128], K - 32[K/32]]$   
SEQUENCE  
FILTER:  $S_1[i, j, k]$   
FILTER:  $S_2[i, j]$

Fig. 13: Tiling with block tile size of  $128 \times 128 \times 32$ .

Fig. 16: Schedule tree transformation for Matmul + Bias + ReLU

matmul with block tile sizes  $128 \times 128 \times 32$  and warp tile sizes  $64 \times 64 \times 32$  with a 2-way intra-thread-block split-K, where the input matrices  $M_0$  and  $M_1$  are in row-major and column major layout respectively. As can be seen the core matmul computation is performed on line 16 through the call to the helper function `hmma_row_col`, which we implement using the `mma.sync.m8n8k4` instructions to realize either a  $16 \times 16 \times 8$  or a  $32 \times 32 \times 8$  macro-MMA. Similarly, the data copy operations are implemented as calls to helper functions.

## VII. KERNEL FUSION

We now discuss how fused kernels can be generated for some computation idioms with both matmul and pointwise operations.

### A. Pointwise Operations in Epilogue

Consider a computation sequence with pointwise operations fed by a matmul e.g. matmul followed by a bias add and ReLU activation, with only the final result being live out. Without loss of generality, all the pointwise operations can be fused together and represented by a single compound operation as in Listing 1. The ISL schedule for this is as shown in Figure 12, which corresponds to the loop-nest shown in Listing 3. The sequence node specifies the relative ordering of the statements that appear in its filter child nodes. Only

DOMAIN :  $S_1[i, j, k] : 0 \leq i < M \wedge 0 \leq j < N \wedge 0 \leq k < K;$   
 $S_2[i, j] : 0 \leq i < M \wedge 0 \leq j < N$

BAND:  $S_1[i, j, k] \rightarrow [[i/128], [j/128]]; S_2[i, j] \rightarrow [[i/128], [j/128]]$   
SEQUENCE  
FILTER:  $S_1[i, j, k]$   
BAND:  $S_1[i, j, k] \rightarrow [[k/32]]$   
BAND:  $S_1[i, j, k] \rightarrow [i - 128[i/128], j - 128[j/128], k - 32[k/32]]$   
FILTER:  $S_2[i, j]$   
BAND:  $S_2[i, j] \rightarrow [[K/32]]$   
BAND:  $S_2[i, j] \rightarrow [i - 128[i/128], j - 128[j/128], K - 32[K/32]]$

Fig. 14: Sequence hoisting for inter-statement dependence.

DOMAIN :  $S_1[i, j, k] : 0 \leq i < M \wedge 0 \leq j < N \wedge 0 \leq k < K \wedge 16[i/16] = i \wedge 16[j/16] = j \wedge 8[k/8] = k; S_2[i, j] : 0 \leq i < M \wedge 0 \leq j < N \wedge 16[i/16] = i \wedge 16[j/16] = j$

BAND:  $S_1[i, j, k] \rightarrow [blockIdx.y, blockIdx.x]; S_2[i, j] \rightarrow [blockIdx.y, blockIdx.x]$   
SEQUENCE  
FILTER:  $S_1[i, j, k]$   
BAND:  $S_1[i, j, k] \rightarrow [[k/32]]$   
BAND:  $S_1[i, j, k] \rightarrow [warpIdx.y, warpIdx.x, 0];$   
BAND:  $S_1[i, j, k] \rightarrow [0, 0, [k/8] - 4[k/32]];$   
BAND:  $S_1[i, j, k] \rightarrow [i - 64[i/64], j - 64[j/64], k - 8[k/8]];$   
FILTER:  $S_2[i, j]$   
BAND:  $S_2[i, j] \rightarrow [[K/32]]$   
BAND:  $S_2[i, j] \rightarrow [warpIdx.y, warpIdx.x, 0];$   
BAND:  $S_2[i, j] \rightarrow [0, 0, [K/8] - 4[K/32]];$   
BAND:  $S_2[i, j] \rightarrow [i - 64[i/64], j - 64[j/64], K - 8[K/8]];$

Fig. 15: Schedule after tiling innermost bands in both the filter nodes with warp-level tile size of  $64 \times 64 \times 32$  and then strip-mining the sequential dimension with strip-size of 8.

the innermost dimensions of band nodes are sequential. Note that unlike in Listing 1, the outer-parallel loops are fused in Listing 3.

As in the case of block-level tiling for just matmul, the band node can be tiled using tile sizes  $b_1 \times b_2 \times b_s$ . Figure 13 shows the result of such a block-tiling. However, given the sequence ordering between statements  $S_1$  and  $S_2$ , it is necessary to hoist the sequence node further up the schedule tree so that all sequential loop dimensions appear only in descendant nodes of the hoisted sequence node. This may require splitting the band members so that the outer parallel loop dimensions fall in a separate band from that of the inner sequential dimensions. Figure 14 illustrates this restructuring. Note that the parent band node of the sequence node only contains parallel loop dimensions. The sequential loop dimensions for the two statements are now moved to separate band nodes immediately under the filter nodes. Such a restructuring ensures that the matmul reduction loop is scheduled before its result is consumed by the pointwise operations.

Clearly, the schedule dimensions constituting the outermost band in Figure 14 correspond to kernel parameters `blockIdx.y` and `blockIdx.x`, as shown in Figure 15. Furthermore, the innermost band under both the filter nodes in Figure 14 iterate over the warp tiles. Consequently, as shown in Figure 15, we can perform warp-tiling and strip-mining on both of these filter



nodes similar to the transformations illustrated in Figure 4 and 6. Schedule domain contraction, as described in Section IV-D is then applied for statement  $S_1$  so that it performs a  $16 \times 16 \times 8$  macro-MMA operation. Similarly, for ease of code generation, the schedule domain of the statement  $S_2$  is also constrained and its operation type updated to one that performs a pointwise operation on an entire accumulator fragment computed by the macro-MMA operation, effectively distributing the pointwise operation across threads.

a) *Avoiding Intermediate Writes To Global Memory*: The schedule space for  $S_1$  is similar to that obtained earlier for matmul alone (see Figure 7). So, similar memory promotions to those described in Section V hold good for this part of the schedule tree. However, since the matmul result is not live-out, the data in an accumulator fragment need not be stored to global memory. Nevertheless, this result is consumed by the pointwise operations scheduled in the other filter node. So, the accumulator data needs to be converted to *fp16* type and then reordered through shared memory, but finally copied back to a register fragment. The reordering ensures that each thread holds a contiguous block of 8 *fp16* values in every register fragment.

b) *Register Fragments for Pointwise Operation*: The register fragments obtained from the accumulator data serve as one of the inputs to the downstream pointwise operation. For the statement  $S_2$ , every other data tile accessed by its warp-level compute tile is promoted to registers e.g. those from access to the `bias` array. These data tiles are similarly distributed across the threads by contracting them by a factor  $16 \times 16$  to obtain an array of register fragments, each containing 8 *fp16* elements. Note that since these fragments have the same data distribution as the register fragments obtained from the accumulator data, they can be loaded from global memory using 128-bit accesses. A copy schedule node is inserted into the schedule tree for the register fragment load operations.

c) *Storing Live-Out to Global Memory*: With all the data tiles accessed by a warp-level compute tile of the pointwise operation distributed across threads into register fragments, the result of the pointwise operation is also in a register fragment. Since it is a contiguous block of 8 *fp16* values, a final copy schedule node is inserted after the pointwise operation to perform a 128-bit store to global memory for each register fragment.

## B. Matmuls with Pointwise Epilogue

Consider the scenario where there are two matmuls of the same shape whose results are consumed by a downstream pointwise operation. The ISL schedule obtained for such an example is shown in Figure 17. The corresponding loop-nest is shown in Listing 4.

Comparing Figures 12 and Figures 17, it is clear that the main structural difference between the schedule trees is that there are three statements involved in the latter and so, three corresponding filter nodes in sequence. Consequently, the same schedule transformations can be applied to obtain a schedule tree similar to that in Figure 15, except that it would

```

DOMAIN :  $S_1[i, j, k] : 0 \leq i < M \wedge 0 \leq j < N \wedge 0 \leq k < K;$ 
          $S_2[i, j, k] : 0 \leq i < M \wedge 0 \leq j < N \wedge 0 \leq k < K;$ 
          $S_3[i, j] : 0 \leq i < M \wedge 0 \leq j < N$ 
BAND:  $S_1[i, j, k] \rightarrow [i, j, k]; S_2[i, j, k] \rightarrow [i, j, k]; S_3[i, j] \rightarrow [i, j, K];$ 
SEQUENCE
FILTER:  $S_1[i, j, k]$ 
FILTER:  $S_2[i, j, k]$ 
FILTER:  $S_3[i, j]$ 

```

Fig. 17: Initial schedule tree for two matmuls feeding an addition.

```

1 for (i = 0; i < M; ++i)
2   for (j = 0; j < N; ++j) {
3     for (k = 0; k < K; ++k) {
4       C[i, j] = mul_acc(C[i, j], A[i, k], B[k, j]); //S1
5       R[i, j] = mul_acc(R[i, j], P[i, k], Q[k, j]); //S2
6     }
7     Z[i, j] = add(C[i, j], R[i, j]); /*S3*/
8   }

```

Listing 4: Sum of Matmuls

have three filter nodes – the first two for the two matmuls and the last one for the pointwise operations, i.e., at the thread-level all of these operations are performed in sequence with no interleaving. Memory promotion presents no additional issues and is handled similarly by avoiding writes of intermediate results to global memory with only the live-out data being stored to it.

In this example, the input matrices to both the matmuls have the same shape. However, the overall approach of tiling for blocks with sequence hoisting to ensure that there is no interleaving of the operations, can be applied even when the input matrices are of different shapes so long as the matmul outputs are of the same shape.

## C. Pointwise Operations in Prologue

Consider the scenario where the matmul inputs are results of pointwise operations as shown in Listing 5. Since each statement is tagged with a specification of its expression tree, the compound operation of ReLU on an input followed by matmul can be represented by a single statement, with matmul as the root in the expression tree.

```

1 for (i = 0; i < M; ++i)
2   for (j = 0; j < N; ++j)
3     for (k = 0; k < K; ++k)
4     /*S1*/C[i, j] = mul_acc(C[i, j], relu(A[i, k]), B[k, j]);

```

Listing 5: ReLU + Matmul

The initial schedule tree for this loop-nest is structurally similar to that in Figure 3. So, all the schedule transformations discussed in Section IV can be applied. This is followed up with memory promotion as discussed in Section V with one crucial difference. Recall that the global-to-shared memory copy is split into a global-to-register copy followed by a register-to-shared copy (see Section V-A). So, all the data that is reused at the block level is first moved to registers. Therefore, when we have pointwise operations in the matmul prologue, instead of moving all this data to shared memory for

reuse, the pointwise operations can be performed on these data values and the result can instead be stored to shared memory for reuse. In effect, even though the compound operation in statement  $S_1$  could have multiple input dataspaces, the shared memory footprint remains the same as that for a matmul without pointwise operations in its prologue. With the pointwise operations being performed during the data movement, the statement  $S_1$  only needs to perform a macro-MMA using two input fragments and an accumulator fragment as in case of a single matmul with no prologue. For the example in Listing 5, the kernel generated would be the same as Listing 2, except that on lines 20 and 21, the result obtained by applying a pointwise ReLU on the 8 *fp16* values which are held in registers, would then be stored to shared memory.

### VIII. EXPERIMENTAL EVALUATION

In this section, we provide an experimental evaluation of the techniques described in the previous sections. We implemented these techniques in the Diesel DSL framework [17]. Diesel provides a basic front-end for specifying tensor expressions and to extract their polyhedral representation. Input to the compiler backend included various code generation options, namely, block tile sizes, warp tile sizes, choice of macro-MMA ( $16 \times 16 \times 8$  or  $32 \times 32 \times 8$ ).

Automatic tile size selection is beyond the scope of this work. So, for every benchmark, we generated CUDA kernels using our compiler backend for various tile size choices and for both the macro-MMA options. All tile sizes experimented were powers of 2, with 16 being the smallest tile size and 128 being the biggest. The split-K schedule was exercised up to a 4-way split. The average performance of each of these kernels over 100 runs was obtained using *nvprof* for 100 problem sizes that were randomly generated, with problem sizes being multiples of 128 (the largest tile size) upto a size of 4096. For every problem size, we present the best performance obtained using our auto-generated kernels.

Baseline versions of the benchmarks were implemented using cuBLAS 10.1 and cuDNN 7.0. The CUBLAS\_GEMM\_DFALT\_TENSOR\_OP algorithm was chosen to target the tensor cores whereas the pointwise operations for bias addition and ReLU activation were implemented using the *cudaAddTensor* and *cudaActivationForward* APIs exposed by cuDNN. The experimental evaluation was performed on an NVIDIA Quadro GV100 GPU with the Volta microarchitecture. The *nvcc* v10.1 compiler was used to compile all the benchmarks with the options: `-O3 -std=c++11 -use_fast_math -ccbin g++ -arch=compute_70 -code=sm_70 -expt-relaxed-constexpr`.

a) *GEMM*: Figure 18 shows a performance plot of the speedups obtained using the auto-generated kernels for GEMM over the *cudaGemmEx* performance. In one in three cases (32%), the auto-generated kernels were able to match or outperform the baseline version. The peak speedup obtained was  $1.75\times$  while it was  $0.78\times$  in the worst case. For 60 of the 100 problem sizes, the speedup was  $0.9\times$  or higher and the geometric mean speedup was  $0.985\times$ .

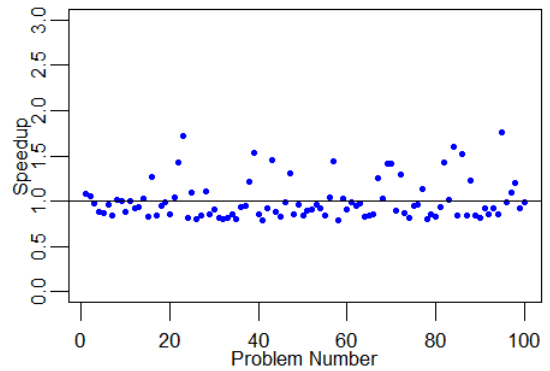


Fig. 18: Performance for GEMM.

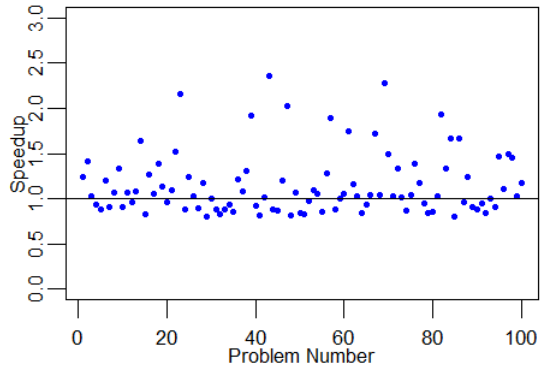


Fig. 19: Performance of prologue fusion: (ReLU + GEMM).

b) *ReLU + GEMM*: In this benchmark, a ReLU pointwise activation function is applied on an input matrix to GEMM. The auto-generated kernel fuses the ReLU in the GEMM prologue and the matmul operation into the same device function. Figure 19 shows a performance plot of the speedups obtained using the auto-generated kernels for GEMM over the baseline, which uses *cudaGemmEx* for performing the GEMM and *cudaActivationForward*. For 61 problem sizes, the auto-generated kernels performed at least as well as the baseline version. The peak speedup obtained was  $2.36\times$  with  $0.80\times$  in the worst case. The geometric mean speedup was  $1.113\times$ . Since the fused kernel is similar to that for GEMM, except that the ReLU operation is performed on registers during the data transfer from global to shared memory, the best tile sizes for the fused kernel correlated with that for GEMM.

c) *GEMM + Bias + ReLU*: A performance plot of the speedups obtained using the fused kernels that were auto-generated for Gemm + Bias + ReLU are shown in Figure 20. Compared to Figure 18, clearly, kernel fusion moves most of the speedups over the baseline, with the auto-generated kernels outperforming the baseline in 94 out of 100 cases. The peak speedup obtained was  $2.55\times$  with  $0.89\times$  being the worst case speedup, with a mean speedup of  $1.29\times$ .

d) *Add(GEMM, GEMM)*: In this benchmark, the results of two GEMMs of the same shape were fed to an add

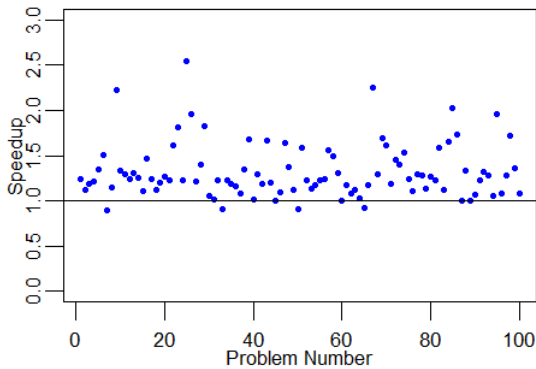


Fig. 20: Epilogue fusion performance: GEMM + Bias + Relu.

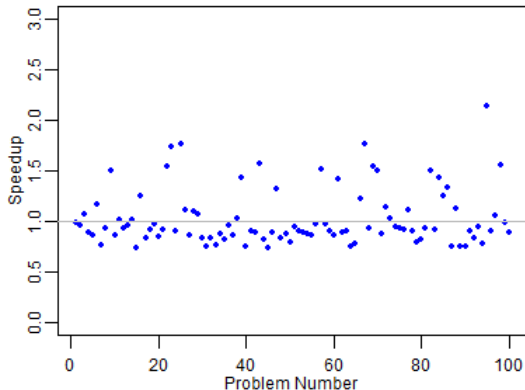


Fig. 21: Kernel fusion performance for Add(GEMM, GEMM).

operation. Figure 21 shows a plot of the speedups obtained through a fused kernel over a baseline that used cuBLAS for gemm and cuDNN for the add operation. For 33 out of the 100 problem sizes, the fused kernel matches or beats the baseline with  $2.13\times$  peak speedup. The worst case speedup is  $0.73\times$ . Overall, with multiple matmuls being fused into the kernel, we noticed there was greater register pressure compared to the other fused kernels, necessitating the use of smaller tiles which while decreasing register pressure were not necessarily optimal for the matmul computation in the fused kernel.

## IX. RELATED WORK

CUDA libraries such as cuBLAS [1] and cuDNN [3] provide highly tuned GPU-accelerated implementations of standard basic linear algebra routines and deep learning primitives. Cutlass [2] is a CUDA C++ template library which provides performance that is comparable to cuBLAS. It features various compute decomposition and data movement strategies for implementing GEMM, with mixed-precision computation support for Volta tensor cores. The tensor core operations in Cutlass are also implemented using the mma instruction. cuTensor [18] is a recent high-performance CUDA library for GPUs with compute capability greater than or equal to 70. It supports various tensor operations such as tensor

contractions, pointwise operations with support for pointwise operator fusion.

Polyhedral compilation has been a topic of active research for several decades [19], [20]. With a large suite of tools and libraries [21]–[25], it has gradually been incorporated into production compilers such as RStream [26], GCC/Graphite [27], LLVM/Polly [28].

Domain specific languages such as Polymage [29] exploit the sophisticated transformation and code generation capabilities of the polyhedral framework to automatically generate high performance implementations of image processing applications. Our work is based on the Diesel DSL compiler framework developed by Elango et al [17], who also tackled the problem of efficient CUDA kernel generation for matmul and some epilog fusion scenarios. However, their focus was more on generating efficient kernels that target traditional CUDA cores. We build on their work to not only target tensor cores but also cover a wider range of computation sequences. Other DSL compiler frameworks such as Halide [16], TVM [30], which are non-polyhedral, separate the notion of the tensor computation from that of its schedule. Tiramisu [31], a polyhedral framework to generate high performance code for GPUs also features a scheduling language to provide low-level control over the schedule to the user. However, the schedule primitives for exploiting tensor cores are limited or primarily rely on the CUDA wmma API for programming them directly [32].

Vasilache et al developed Tensor Comprehensions (TC) [33], [34], which leverages the Halide compiler [16] in conjunction with polyhedral compilation to automatically generate CUDA kernels given a mathematical specification of a deep learning graph. It uses a modified version of the PPCG compiler developed by Verdoolaege et al [9] with support for operator fusion. While TC handles a larger class of affine loop-nests, we deal with kernel generation for tensor cores with a focus on a few common computation idioms. Zerrell et al [35] developed Stripe, a nested polyhedral intermediate representation used in the PlaidML [36] compiler with the facility to fuse tensor contractions. MLIR [12] is an ongoing project which aims to unify the compiler infrastructure for machine learning by providing the ability to embed multiple IR dialects in it e.g. linear algebra dialect or an affine dialect, with a progressive lowering and transformation of IR dialects. Overall, we believe our work is complementary and could be integrated with many of these frameworks as a library for targeting tensor cores.

## X. CONCLUSION

We tackled the problem of automatic generation of efficient CUDA kernels for computation sequences involving matmul and pointwise operations. To the best of our knowledge, this is the first work to leverage polyhedral compilation techniques for exploiting tensor core capabilities on a Volta GPU. In particular, we relied upon macro-MMA compositions of size  $16\times 16\times 8$  and  $32\times 32\times 8$  implemented using the *mma.sync.m8n8k4* PTX instruction for targeting tensor cores.

Furthermore, we demonstrated that these techniques can lead to significant speedups for a wide range of problem sizes. In the future, we intend to augment this approach with cost models for automatic tile size selection as well as generalize it for subsequent GPU micro-architectures such as Turing.

#### ACKNOWLEDGMENT

We thank all contributors to the Diesel compiler – Venmugil Elango, Mahesh Ravishankar, Norm Rubin, for creating the framework in which we could try out the ideas described in this paper. We also thank Bastian Hagedorn for his comments on leveraging the mma instructions for targeting Volta tensor cores.

#### REFERENCES

- [1] NVIDIA, “cublas,” 2019, <https://docs.nvidia.com/cuda/cublas/index.html>.
- [2] —, “Cuda templates for linear algebra subroutines,” 2019, <https://github.com/NVIDIA/cutlass>.
- [3] S. Chetlur, C. Woolley, P. Vandermersch, J. Cohen, J. Tran, B. Catanzaro, and E. Shelhamer, “cudnn: Efficient primitives for deep learning,” *CoRR*, vol. abs/1410.0759, 2014. [Online]. Available: <http://arxiv.org/abs/1410.0759>
- [4] M. Abadi, P. Barham, J. Chen, Z. Chen, A. Davis, J. Dean, M. Devin, S. Ghemawat, G. Irving, M. Isard, M. Kudlur, J. Levenberg, R. Monga, S. Moore, D. G. Murray, B. Steiner, P. A. Tucker, V. Vasudevan, P. Warden, M. Wicke, Y. Yu, and X. Zheng, “Tensorflow: A system for large-scale machine learning,” in *12th USENIX Symposium on Operating Systems Design and Implementation, OSDI 2016, Savannah, GA, USA, November 2-4, 2016*, 2016, pp. 265–283. [Online]. Available: <https://www.usenix.org/conference/osdi16/technical-sessions/presentation/abadi>
- [5] A. Paszke, S. Gross, F. Massa, A. Lerer, J. Bradbury, G. Chanan, T. Killeen, Z. Lin, N. Gimeshein, L. Antiga, A. Desmaison, A. Köpf, E. Yang, Z. DeVito, M. Raison, A. Tejani, S. Chilamkurthy, B. Steiner, L. Fang, J. Bai, and S. Chintala, “Pytorch: An imperative style, high-performance deep learning library,” in *Advances in Neural Information Processing Systems 32: Annual Conference on Neural Information Processing Systems 2019, NeurIPS 2019, 8-14 December 2019, Vancouver, BC, Canada*, 2019, pp. 8024–8035. [Online]. Available: <http://papers.nips.cc/paper/9015-pytorch-an-imperative-style-high-performance-deep-learning-library>
- [6] NVIDIA, “Cuda toolkit documentation,” 2019, <https://docs.nvidia.com/cuda/parallel-thread-execution/index.html#warp-level-matrix-fragment-mma-884>.
- [7] —, “Programming tensor cores in cuda 9,” 2017, <https://devblogs.nvidia.com/programming-tensor-cores-cuda-9/>.
- [8] U. Bondhugula, A. Hartono, J. Ramanujam, and P. Sadayappan, “A practical automatic polyhedral program optimization system,” in *PLDI*, Jun 2008.
- [9] S. Verdoolaege, J. C. Juega, A. Cohen, J. I. Gómez, C. Tenllado, and F. Catthoor, “Polyhedral parallel code generation for CUDA,” *TACO*, vol. 9, no. 4, pp. 54:1–54:23, 2013. [Online]. Available: <https://doi.org/10.1145/2400682.2400713>
- [10] M. Baskaran, U. Bondhugula, S. Krishnamoorthy, J. Ramanujam, A. Rountev, and P. Sadayappan, “A Compiler Framework for Optimization of Affine Loop Nests for GPGPUs,” in *ACM Intl. conference on Supercomputing (ICS)*, Jun. 2008.
- [11] N. Vasilache, O. Zinenko, T. Theodoridis, P. Goyal, Z. DeVito, W. S. Moses, S. Verdoolaege, A. Adams, and A. Cohen, “Tensor comprehensions: Framework-agnostic high-performance machine learning abstractions,” *CoRR*, vol. abs/1802.04730, 2018. [Online]. Available: <http://arxiv.org/abs/1802.04730>
- [12] C. Latner, J. A. Pienaar, M. Amini, U. Bondhugula, R. Riddle, A. Cohen, T. Shpeisman, A. Davis, N. Vasilache, and O. Zinenko, “MLIR: A compiler infrastructure for the end of moore’s law,” 2020. [Online]. Available: <https://arxiv.org/abs/2002.11054>
- [13] S. V. M. K. R. Schreiber and H. Kamepalli, “Generating simd instructions for cerebras cs-1 using polyhedral compilation techniques,” 2020.
- [14] S. Verdoolaege, “isl: An integer set library for the polyhedral model,” in *Mathematical Software - ICMS 2010, Third International Congress on Mathematical Software, Kobe, Japan, September 13-17, 2010. Proceedings*, 2010, pp. 299–302. [Online]. Available: [https://doi.org/10.1007/978-3-642-15582-6\\_49](https://doi.org/10.1007/978-3-642-15582-6_49)
- [15] S. Verdoolaege, S. Guelton, T. Grosser, and A. Cohen, “Schedule trees,” in *IMPACT*, 01 2014.
- [16] J. Ragan-Kelley, C. Barnes, A. Adams, S. Paris, F. Durand, and S. P. Amarasinghe, “Halide: a language and compiler for optimizing parallelism, locality, and recomputation in image processing pipelines,” in *ACM SIGPLAN symposium on Programming Languages Design and Implementation*, 2013, pp. 519–530.
- [17] V. Elango, N. Rubin, M. Ravishankar, H. Sandanagobalane, and V. Grover, “Diesel: DSL for linear algebra and neural net computations on gpus,” in *Proceedings of the 2nd ACM SIGPLAN International Workshop on Machine Learning and Programming Languages, MAPL@PLDI 2018, Philadelphia, PA, USA, June 18-22, 2018*, 2018, pp. 42–51. [Online]. Available: <https://doi.org/10.1145/3211346.3211354>
- [18] NVIDIA, “cutensor: A high-performance cuda library for tensor primitives,” 2019, <https://docs.nvidia.com/cuda/cutensor/index.html>.
- [19] P. Feautrier, “Some efficient solutions to the affine scheduling problem: Part I, one-dimensional time,” *Intl. Journal of Parallel Programming*, vol. 21, no. 5, pp. 313–348, 1992.
- [20] —, “Some efficient solutions to the affine scheduling problem: Part II, multidimensional time,” *Intl. Journal of Parallel Programming*, vol. 21, no. 6, pp. 389–420, 1992.
- [21] “PLUTO: An automatic polyhedral parallelizer and locality optimizer for multicores,” <http://pluto-compiler.sourceforge.net>.
- [22] “POCC: Polyhedral compiler collection,” <http://pocc.sourceforge.net>.
- [23] “CLOoG: The Chunky Loop Generator,” <http://www.cloog.org>.
- [24] “PIP: The Parametric Integer Programming Library,” <http://www.piplib.org>.
- [25] “The LooPo Project - Loop parallelization in the polytope model,” <http://www.fmi.uni-passau.de/loopo>.
- [26] “RSTREAM - High Level Compiler, Reservoir Labs,” <http://www.reservoir.com>.
- [27] S. Pop, A. Cohen, C. Bastoul, S. Girbal, G. Silber, and N. Vasilache, “Graphite: Loop optimizations based on the polyhedral model for gcc,” 2006.
- [28] T. Grosser, H. Zheng, R. Aloor, A. Simbrger, A. Grolinger, and L.-N. Pouchet, “Polly: Polyhedral optimization in LLVM,” in *IMPACT*, 2011.
- [29] R. T. Mullapudi, V. Vasista, and U. Bondhugula, “Polymage: Automatic optimization for image processing pipelines,” in *Intl. Conference on Architectural Support for Programming Languages and Operating Systems, ser. ASPLOS ’15*, 2015, pp. 429–443.
- [30] T. Chen, T. Moreau, Z. Jiang, L. Zheng, E. Q. Yan, H. Shen, M. Cowan, L. Wang, Y. Hu, L. Ceze, C. Guestrin, and A. Krishnamurthy, “TVM: an automated end-to-end optimizing compiler for deep learning,” in *13th USENIX Symposium on Operating Systems Design and Implementation, OSDI 2018, Carlsbad, CA, USA, October 8-10, 2018*, 2018, pp. 578–594. [Online]. Available: <https://www.usenix.org/conference/osdi18/presentation/chen>
- [31] R. Baghdadi, J. Ray, M. B. Romdhane, E. D. Sozzo, A. Akkas, Y. Zhang, P. Suriana, S. Kamil, and S. P. Amarasinghe, “Tiramisu: A polyhedral compiler for expressing fast and portable code,” in *IEEE/ACM International Symposium on Code Generation and Optimization, CGO 2019, Washington, DC, USA, February 16-20, 2019*, 2019, pp. 193–205. [Online]. Available: <https://doi.org/10.1109/CGO.2019.8661197>
- [32] “How to optimize convolution using tensorcores,” 2018, [https://docs.tvm.ai/tutorials/optimize/opt\\_conv\\_tensorcore.html](https://docs.tvm.ai/tutorials/optimize/opt_conv_tensorcore.html).
- [33] N. Vasilache, O. Zinenko, T. Theodoridis, P. Goyal, Z. DeVito, W. S. Moses, S. Verdoolaege, A. Adams, and A. Cohen, “The next 700 accelerated layers: From mathematical expressions of network computation graphs to accelerated GPU kernels, automatically,” *TACO*, vol. 16, no. 4, pp. 38:1–38:26, 2020. [Online]. Available: <https://doi.org/10.1145/3355606>
- [34] —, “Tensor comprehensions: Framework-agnostic high-performance machine learning abstractions,” *CoRR*, vol. abs/1802.04730, 2018. [Online]. Available: <http://arxiv.org/abs/1802.04730>
- [35] T. Zerrell and J. Bruestle, “Stripe: Tensor compilation via the nested polyhedral model,” *CoRR*, vol. abs/1903.06498, 2019. [Online]. Available: <http://arxiv.org/abs/1903.06498>
- [36] Intel, “Plaidml,” 2019,

---

<https://www.intel.ai/plaidml>.